Two-Dimensional Correlation Spectroscopy Reveals Coupled Immunoglobulin Regions of Differential Flexibility that Influence Stability

Tim J. Kamerzell and C. Russell Middaugh*

Department of Pharmaceutical Chemistry, University of Kansas, Lawrence, Kansas 66047

Received April 4, 2007; Revised Manuscript Received June 5, 2007

ABSTRACT: Despite the well-accepted importance of protein flexibility and dynamics in molecular recognition and conformational stability, our understanding of these relationships is incomplete. Immunoglobulin flexibility is essential for antigen binding and adaptation to diverse molecular shapes and sizes. The inherent flexibility of immunoglobulins also renders these molecules suitable for investigating the possible relationships between protein flexibility and stability. To better understand these inter-relationships, we employ generalized perturbation-based two-dimensional correlation FTIR spectroscopy to monitor the time evolution of H−D exchange of an IgG1 as a function of pH. The differential flexibility of various immunoglobulin regions is described in response to an external perturbation and shown to vary widely. The greatest number of regions with differential exchange rates and, thus differential flexibility, is seen at pH 6. Approximately seven, six, five, and four separate states that exchange with different rates were observed at pH 6, 8, 4, and 2, respectively. The overall distribution of exchange rates calculated from the decays of the integrated Amide I and Amide II areas provides further evidence of multiple regions with differential flexibility. The sequence of events at pH 4 determined from the asynchronous vibrational patterns is of significant interest and suggests protonation of Glu and Asp side chains occurs first and initiates changes in the conformation and flexibility of different sheet and turns structure. A complex inter-relationship between differential regional flexibility and conformational coupling (i.e., cooperativity) initiated by changes in pH influences the stability of this IgG.

The current view of proteins as statistical distributions of conformational microstates with regions of differential flexibility and various internal motions is now beginning to shape our understanding of molecular recognition events, cellular communication, and protein stability. Coupled domain motions, correlated dynamics across extended structures, concerted fluctuations, vibrational oscillations, and local and global unfolding equilbria contribute to a complicated inter-relationship among protein flexibility, stability, and biological function (*1*−*6*). Although our knowledge of these relationships is improving at a rapid rate, direct relationships among protein flexibility, stability, and function are only beginning to be understood.

Immunoglobulins are involved in a wide range of biological activities, including antigen binding, complement fixation, and secondary effector functions. Four disulfide-linked chains comprise the fundamental framework of all immunoglobulins which consists of two heavy and two light chains. The light and heavy chains may be further divided into variable and constant regions and make up antigen binding (Fab) and crystallizable fragments (Fc). The Fab and Fc units are connected by a flexible hinge region which is thought to be responsible for much of the dynamic behavior of immunoglobulins. Immunoglobulin G (IgG) functions are critically dependent on the flexibility of the molecule. Diverse internal motions of IgG regulate antigen and complement binding as well as cell membrane interactions. Various aspects of the flexibility of immunoglobulin G (IgG)[1] molecules have been characterized using fluorescence anisotropy (*7*−*9*) and resonance energy transfer (*10*), multidimensional nuclear magnetic resonance spectroscopy (NMR) (*11*, *12*), X-ray, and neutron scattering (*13*) among other methods. In general, these methods have shown that IgG flexibility is greatest in the hinge region and one Fc C_{H2} domain, while the Fab arms are able to freely rotate around a connecting hinge region with extreme asymmetry.

All immunoglobulin chains consist of small compact domains of a bilayer of β-sheet stabilized by an intrachain disulfide bond. Despite the similarity in structure and sequence homology of a single subclass of IgG molecules, their stabilities can vary widely. The observed diversity of IgG functions and stabilities may be due to differences in their flexibility, conformational fluctuations, and dynamics. Thus, a better understanding of the differences in the flexibility and dynamics of these molecules should help us to better understand their behavior.

NMR currently is the method of choice for studying protein motions over a broad range of time scales and amplitudes. Nuclear spin relaxation techniques, including measurements of multiple quantum relaxation processes, have significantly advanced our understanding of the correlated and uncorrelated dynamics of protein molecules (*14*). The

* To whom correspondence should be addressed: Department of Pharmaceutical Chemistry, University of Kansas, 2030 Becker Dr., Lawrence, KS 66047. Telephone: (785) 864-5813. Fax: (785) 864-5814. E-mail: Middaugh@ku.edu.

[1] Abbreviations: IgG, immunoglobulin G; mAb, monoclonal antibody.

10.1021/bi700645k CCC: $37.00
Published on Web 08/03/2007

large size of immunoglobulin molecules (~150 kDa) has primarily limited applications of this approach to Ig fragments. Every method, however, has its limitations, and complementary measurments of protein flexibility and dynamics are necessary to provide a comprehensive picture of protein dynamic processes.

Two-dimensional correlation spectroscopy, proposed in 1986 by Noda, holds significant promise for advancing our understanding of the relationships between protein flexibility and stability (*15*, *16*). Through application of cross-correlation and statistical analyses, this method monitors the selective changes in spectral intensity variations as a function of two different spectral variables as a result of application of an external perturbation. By monitoring these changes, we may obtain a wide range of information depending on the choice of spectroscopic probe and external perturbation. Asynchronous correlation spectroscopy is of particular interest because of its resolution and ability to elucidate the sequence of events giving rise to patterns of spectral intensity variations (*17*). Likewise, hybrid or heterocorrelation spectroscopy uses multiple types of perturbations and can elucidate differences in patterns of spectral intensity variations resulting from these perturbations (*18*). These methods have been previously established and applied to a variety of proteins. The purpose of this work is to apply this powerful approach for the first time to an IgG molecule.

The exchange of protein backbone amide protons with deuterium provides information about protein flexibility, conformational distributions, hydrogen bonding patterns, and structure (*19*−*21*). The numerous methods used to follow the time course of exchange include NMR, mass spectrometry, and FTIR spectroscopy. Combined with the use of time series and cross-correlation analysis, FTIR H−D exchange experiments can provide a wealth of information concerning the flexibility of different regions within a protein (*22*). Furthermore, the deconvolution power of asynchronous two-dimensional (2D) correlation spectroscopy enables the separation of differential exchange rates between regions of the same and different secondary structural elements.

In this study, we investigate the differential flexibility of a monoclonal antibody from a sequence of H−D exchange events as a function of pH using 2D correlation and heterocorrelation FTIR spectroscopy. The differential flexibility of immunoglobulin regions is described in response to an external perturbation and shown to vary widely. The sequence of events at each pH was determined from the asynchronous vibrational patterns, suggesting a complex inter-relationship between differential flexibility and conformational coupling initiated by changes in pH influences the stability of this IgG.

EXPERIMENTAL PROCEDURES

Immunoglobulin G1 containing a κ light chain (IgG1κ), monoclonal antibody (mAb) was kindly provided by MedImmune, Inc. (Gaithersburg, MD), and stored in its formulation buffer at 2−8 °C. All chemicals were of reagent grade and were obtained from Sigma (St. Louis, MO) and Fisher Scientific (Pittsburgh, PA). All solutions were prepared in 20 mM citrate, 20 mM phosphate buffer, with an ionic strength of ~0.15 adjusted with NaCl (pH 2.00, 4.00, 6.00, and 8.00), and dialyzed overnight. Protein concentrations were determined at room temperature by absorbance measurement at 280 nm (ϵ = 1.5 mL mg^{-1} cm^{-1}) using an Agilent (Palo Alto, CA) 8453 UV−visible spectrophotometer fitted with a Peltier temperature controller. D_2O buffers were prepared in the same manner as described above, and the pD was determined as the pH reading + 0.44.

Fourier Transform Infrared Spectroscopy (FTIR). Infrared spectra were recorded at 25 °C using an attenuated total internal reflectance (ATR) accessory mounted in a BOMEM (Quebec, QC) MB-104 FTIR spectrometer at a resolution of 4 cm^{-1}. The spectrometer and sample trough were continuously purged with dry air, which was controlled using two flow meters. A Thermal A.R.K. temperature controller (Spectra-Tech, Shelton, CT) and zinc selenide (ZnSe) crystal with a 45° incidence angle were used. Aqueous mAb solutions and D_2O buffer were incubated separately at 25 °C prior to dilution. Concentrated stock dialyzed mAb solutions (100 mg/mL) were then diluted with D_2O buffer to a final concentration of 10 mg/mL mAb (90% D_2O), and spectra were immediately recorded. Data were collected for >10 h with 1700 time-resolved subfiles and seven scans per subfile. The reference buffer was measured using the same parameters and conditions, and each corresponding time point was subtracted from the protein spectra. After subtraction, a seven-point, second-degree polynomial Savitzky−Golay smoothing filter was applied to the spectra.

Two-Dimensional Correlation Spectroscopy. In this work, FTIR spectroscopy was used to monitor the evolution of H−D exchange of an IgG and the subsequent spectral intensity variations along the time and frequency axis. An additional external perturbation of pH (2, 4, 6, and 8) was used to modulate stability and flexibility. Matrices of m rows of spectral traces and n columns of spectral intensity variations were created from the time-dependent FTIR spectra. From each matrix, the synchronous and asynchronous spectra, covariance, statistical correlation coefficient, and hybrid correlation matrices were calculated.

The synchronous correlation spectrum represents the similarity of spectral intensity variations at two different wavenumbers along the time axis of deuterium exchange (*17*). Correlation peaks arise along the diagonal and off-diagonal (cross-peaks) positions of the synchronous spectrum due to changes in the spectral intensity variations. This is mathematically equivalent to the autocorrelation or variance. The cross-peaks represent simultaneous changes in spectral intensity at two separate wavenumbers and can be positive or negative. The sign of the cross-peaks defines the behavior of the spectral intensity. For example, a positive cross-peak implies that the intensity variations are changing in a similar way (ν_1 and ν_2 decreasing or increasing together), while a negative cross-peak means that the intensity variations are changing in opposite directions (ν_1 increasing and ν_2 decreasing). Each set of IR spectra may be represented as a dynamic set of spectra in time (t) by

$$\tilde{y}_j(\nu) = \tilde{y}_j(\nu,t)$$

where ν is the wavenumber and the jth point in time is given by $t_j = T_{min} + [(T_{max} - T_{min})(j - 1)]/(m - 1)$, where m is the number of equally spaced time points (*16*, *17*). The reference spectrum (average spectrum) was subtracted from the initial data as is common practice. The synchronous 2D

correlation intensity $\Phi(\nu_1,\nu_2)$, which represents the simultaneous changes of two separate spectral intensity variations at ν_1 and ν_2, may then be obtained from the relationship

$$\Phi(\nu_1,\nu_2) = \frac{1}{m-1}\sum_{j=1}^{m}\tilde{y}_j(\nu_1)\tilde{y}_j(\nu_2)$$

The discrete data collected from the IR measurements were represented in matrix notation as previously described by Noda (*23*):

$$\mathbf{Y} = \begin{bmatrix} \tilde{y}(\nu_1,t_1) & \tilde{y}(\nu_2,t_1) & \cdots & \tilde{y}(\nu_n,t_1) \\ \tilde{y}(\nu_1,t_2) & \tilde{y}(\nu_2,t_2) & \cdots & \tilde{y}(\nu_n,t_2) \\ \cdots & \cdots & \cdots & \cdots \\ \tilde{y}(\nu_1,t_m) & \tilde{y}(\nu_1,t_m) & \cdots & \tilde{y}(\nu_n,t_m) \end{bmatrix}$$

where $\tilde{y}(\nu,t)$ is the set of dynamic spectra, from which the synchronous 2D correlation spectrum is defined as the inner product where each column of the matrix **Y** is a vector:

$$\Phi(\nu_1,\nu_2) = \frac{1}{m-1}\tilde{y}(\nu_1)^T\tilde{y}(\nu_2) \text{ or } \Phi = \frac{1}{m-1}\mathbf{Y^T}\cdot\mathbf{Y}$$

(covariance matrix)

It has also been shown that the synchronous spectrum is similar to the covariance matrix if the measurements are recorded at fixed intervals (*23*). The covariance matrix (**C**) of n sets of variates (X_1, ..., X_n) was calculated and defined as

$$\mathbf{C}_{ij}^{mn} = \langle (x_i - \mu_i)^m (x_j - \mu_j)^n \rangle$$

where μ_i is the mean. The diagonal elements of the covariance matrix represent the autocorrelation of intensity variations with time at a given wavenumber, and the cross-peaks indicate the simultaneous change in intensity between wavenumbers.

The matrix (**R**) of statistical correlation coefficients is related to the covariance matrix **C**(i,j) and was calculated from the well-known relationship

$$\mathbf{R}(i,j) = \frac{\mathbf{C}(i,j)}{\sqrt{\mathbf{C}(i,i)\cdot\mathbf{C}(j,j)}}$$

where **C**(i,i) and **C**(j,j) are elements of the covariance matrix. The correlation coefficients are a normalized (−1 to 1) measure of the strength of the relationships between two variables, where a value of 1, −1, or 0 means that there is positive, negative, or no relationship between the variables, respectively.

The asynchronous correlation spectrum $\Psi(\nu_1,\nu_2)$, which represents the dissimilarity of spectral variations as a function of deuterium exchange time can be represented in matrix notation and defined as

$$\Psi(\nu_1,\nu_2) = \frac{1}{m-1}\tilde{y}(\nu_1)^T N\tilde{y}(\nu_2) \text{ or } \Psi = \frac{1}{m-1}\mathbf{Y^T}\cdot\mathbf{N}\cdot\mathbf{Y}$$

where **N** is the Hilbert−Noda transformation matrix (*17*). The asynchronous spectrum is antisymmetric, and cross-peaks arise only if the spectral intensity variations change out of phase with each other. Thus, the asynchronous spectrum is useful for interpreting the sequential order of spectral intensity variations.

The differences in spectral intensity variations between the data matrices as a function of pH may be obtained from the hybrid 2D correlation method (*18*, *24*). The synchronous hybrid correlation spectrum was constructed from the two data matrices $\mathbf{Y}_1$ and $\mathbf{Y}_2$ (pH 2 vs pH 4, pH 2 vs pH 6, etc.) using the relationship

$$\Phi(\nu_1,\nu_2) = \frac{1}{m-1}\mathbf{Y}_1^{\mathbf{T}}\cdot\mathbf{Y}_2$$

It should be noted that the sample number in the two matrices is equal.

The ability to discriminate between correlation peaks due to artifacts and those due to true correlation peaks is critical in the analysis of perturbation-based 2D correlation spectroscopy. In attempts to rule out artifactual correlation peaks, the ratio of asynchronous to synchronous functions, $F(\nu_1,\nu_2)$, has been determined following the method proposed by Buchet et al. (*25*) using the relationship

$$F(\nu_1,\nu_2) = \Psi(\nu_1,\nu_2)/\Phi(\nu_1,\nu_2)$$

This ratio has been suggested to be a measure of the degree of coherence similar to the global correlation phase angle proposed by Noda (*26*). It has also been shown that in the case of an exponential decaying perturbation (e.g., isotope exchange), $F(\upsilon_1,\upsilon_2)$ is not associated with a difference phase angle but rather reflects the degree of correlation between rate constants $k(\upsilon_1)$ and $k(\upsilon_2)$ of the two bands υ_1 and υ_2 (*25*, *27*).

The covariance and statistical 2D correlation matrices were calculated and plotted using routine functions in Matlab version 7.1. Synchronous and asynchronous correlation spectra were calculated using three separate programs: (I) Matlab, (II) 2Dshige version 1.3 developed by Morita (*28*), and (III) an integrated Matlab program kindly provided by E. Goormaghtigh (*29*). The synchronous and asynchronous correlation spectra were compared and verified using the different programs. The final analysis, graph construction, and matrix manipulation used Matlab version 7.1.

Hydrogen−Deuterium Exchange Rates. The ratio of the Amide II/Amide I area was determined by direct integration and used to calculate the distribution of rate constants of exchange. The number of exchange sites (N) is assumed to follow first-order kinetics according to the following sum:

$$H_R(t) = \sum_{j=1}^{N}\exp(-k_j t)$$

where H_R is the number of hydrogens remaining unexchanged. To compute the distribution shape, the sum is replaced by an integral as described by Knox and Rosenberg (*30*):

$$H_R(t) = \int_0^\infty f(k)e^{-kt}\,dk$$

The time-dependent behavior of the number of hydrogens remaining unexchanged is represented as the Laplace transform of the distribution function $f(k)$, and the distribution of

rate constants is obtained from the inverse Laplace transform of the remaining unexchanged hydrogens:

$$f(k) = L^{-1}H_R(t)$$

The integrated Matlab program KINETICS provided by the Goormaghtigh lab was used to express the decay as a continuous distribution of time constants $f(k)$ using the method described by Knox and Rosenberg (*30*). The program CONTIN, as a part of the KINETICS program, was used to solve the inverse Laplace transform as previously described (*31*, *32*).

RESULTS

Second-Derivative FTIR Spectra

The second-derivative IR spectra of the mAb as a function of exchange time and pH were used to assess the component bands contributing to the Amide I region. These were then compared to the two-dimensional spectra (Figure 1A−D). The predominant bands at pH 2 at times of <1 min are located at 1637, 1662, 1670, and 1689 cm^{-1}, corresponding to the expected principal secondary structural elements of β-sheet (1637 and 1670 cm^{-1}) and turns (1660 and 1689 cm^{-1}). After long exchange times, a band at 1628 cm^{-1} appears that may be assigned to short irregular extended structure or aggregated β-strands. This band was not present in the second-derivative spectrum for the mAb at any other pH. The minima of the second-derivative spectra at pH 4 and times of <1 min are located at 1639, 1664, 1680, and 1689 cm^{-1}. Subtle shifts of the 1639 and 1676 cm^{-1} bands of 2 and 4 cm^{-1} were observed after 10 h at pH 4. The band assignments and locations of the second-derivative peaks at pH 6 were 1612, 1637, 1664, 1676, and 1690 cm^{-1} at times of <1 min and 1612, 1637, 1668, and 1686 cm^{-1} at times of >10 h. The minima of the second-derivative spectra at pH 8 are found at 1609, 1637, 1668, and 1688 cm^{-1} at short times and 1605, 1636, 1664, 1674, and 1686 cm^{-1} at longer exchange times.

Two-Dimensional Correlation Spectroscopy

Covariance Matrices and Synchronous Spectra. The development of perturbation-based 2D correlation spectroscopy was first described by Noda in 1986 (*15*−*17*) and expanded in later years to a more broad-based application now known as generalized 2D correlation spectroscopy (*23*, *27*). In this work, the synchronous correlation spectrum represents the similarity of spectral intensity variations at two different wavenumbers along the time axis of deuterium exchange. Correlation peaks arise along the diagonal and off-diagonal (cross-peaks) positions of the synchronous spectrum. Mathematically, the autocorrelation or variance of spectral intensity is present along the diagonal. The cross-peaks represent simultaneous changes in spectral intensity at two different wavenumbers and may be positive or negative. The sign of the cross-peak defines the behavior of the spectral intensity variations. For example, a positive cross-peak implies that the intensity variations at frequency 1 (ν_1) and frequency 2 (ν_2) are changing in a similar way (e.g., decreasing or increasing together), while a negative cross-peak indicates that the intensity variations are changing in opposite directions (e.g., ν_1 increasing and ν_2 decreasing).

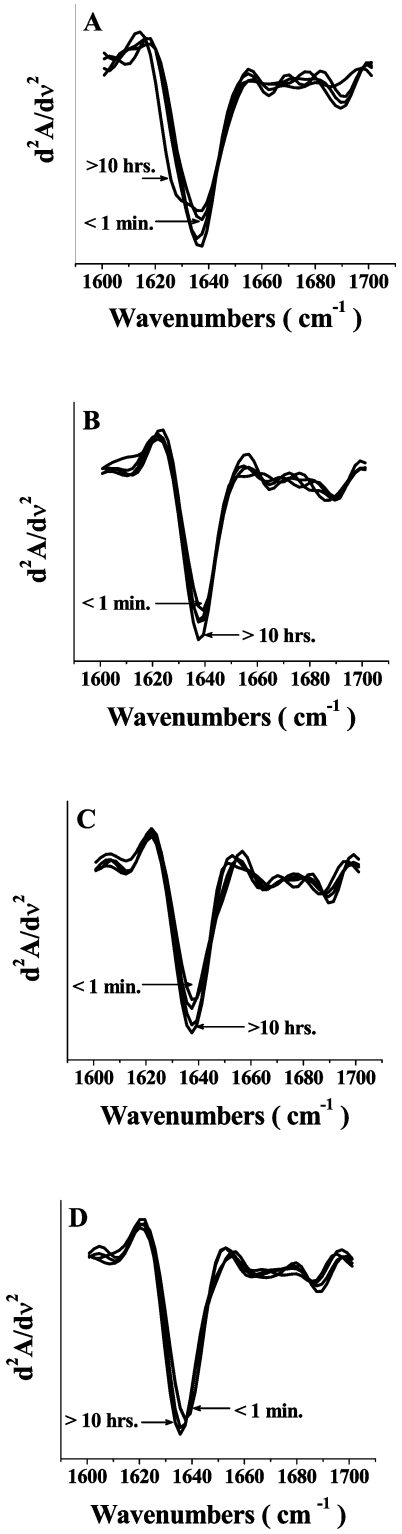

FIGURE 1: Second-derivative FTIR spectra of the Amide I band at exchange times of less than 1 min and greater than 10 h for the mAb at pH (A) 2, (B) 4, (C) 6, and (D) 8.

Covariance maps are a symmetric square matrix mathematically equivalent to the synchronous correlation spectra and are shown for the mAb as a function of pH in Figure 2. The diagonal elements (autopeaks) represent the variance of spectral signal fluctuations as a function of time for the representative spectral variable, while the cross-peaks correspond to the covariance between spectral signal fluctuations at two separate spectral variables.

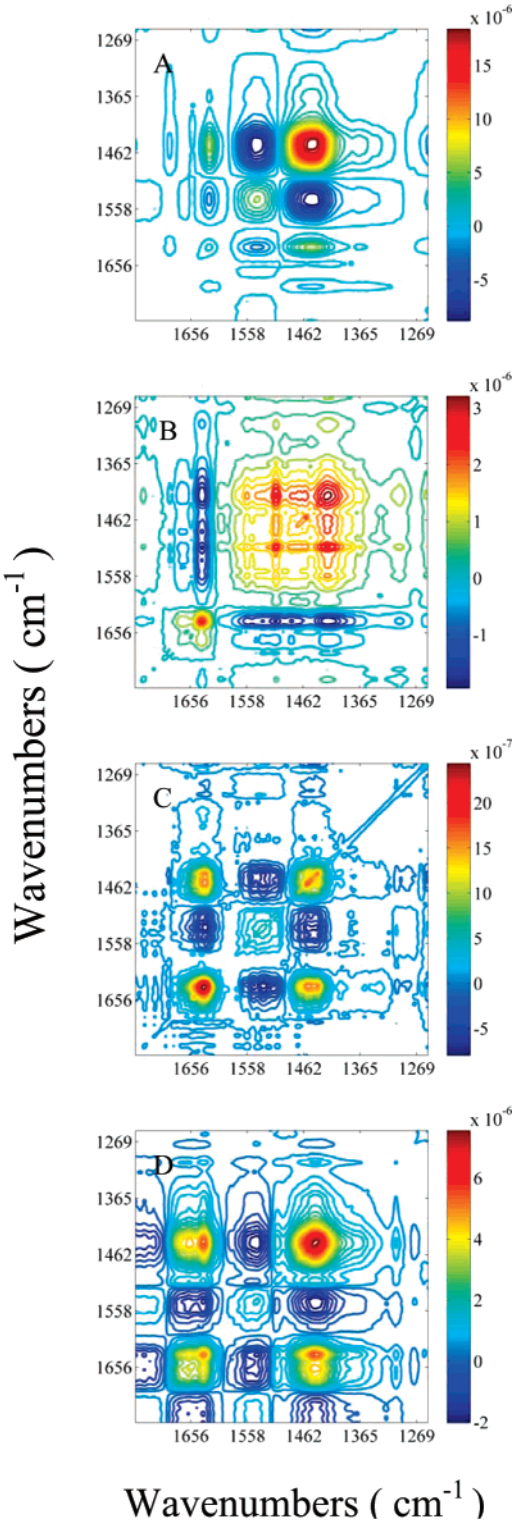

FIGURE 2: IgG covariance maps of the spectral signal fluctuations corresponding to the frequency range of 1750−1250 cm^{-1} at pH (A) 2, (B) 4, (C) 6, and (D) 8. The scaled intensity change is shown in color from negative to positive from blue to red.

Autopeaks along the diagonal of the covariance map are located at 1450, 1543, and (1624, 1662) cm^{-1} for the mAb at pH 2 (Figure 2A). The peak at (1624, 1662) cm^{-1} is a combination Amide I band with overlapping contributions, which are not well-resolved. The strongest autopeak at 1450 cm^{-1} is due to the increasing magnitude of the Amide II′ band, while the relatively weak peak at 1543 cm^{-1} corresponds to the decreasing magnitude of the Amide II signal. The cross-peaks of the Amide I band are assigned to β-sheet or extended aggregated strand (1624 cm^{-1}), turns/disordered structure (1653 cm^{-1}), β-sheet/turns (1684 cm^{-1}), and turns (1691, 1666 cm^{-1}).

The diagonal peaks at pH 4 correspond to the Amide II′, Amide II, and Amide I bands, respectively (Figure 2B). A considerable degree of line broadening is seen for the Amide II band at 1510 cm^{-1} which is easily detected from the four-way symmetric pattern and the negative vertical cross-peaks in the asynchronous spectrum. At this pH, the Amide I band cross-peaks represent β-sheet (1636 cm^{-1}) and turns (1666 cm^{-1}).

The strongest autopeak for the mAb at pH 6 is seen at 1635 cm^{-1}, followed by an intermediate peak at 1452 and a relatively weak band near 1529 cm^{-1} (Figure 2C). Again, these three autopeaks correspond to the Amide I, II′, and II bands, respectively. Corresponding cross-peaks arise at the coordinates (1635, 1684), (1568, 1454), (1635, 1568), and (1641, 1261) cm^{-1}. β-Sheet, disordered, and β-sheet/turn structures are assigned to the coordinates at 1635, 1641, and 1684 cm^{-1}, respectively.

The autopeaks for the IgG at pH 8 are located at 1443, 1545, 1634, and 1659 cm^{-1} (Figure 2D). The strongest band at 1443 cm^{-1} is slightly broadened, while the Amide I peak is composed of multiple overlapping signals. Cross-peaks arise from the signal fluctuations corresponding to the vibrational bands at 1634 and 1657−1659 cm^{-1} and represent β-sheet and turns at pH 8, respectively. The synchronous correlation spectra for the mAb at pH 2, 4, 6, and 8 are identical to the covariance maps and were used only for comparative purposes (data not shown).

Asynchronous Correlation Spectra. The asynchronous correlation spectra are powerful tools for the deconvolution of overlapping vibrational bands and enable a more critical analysis of the order of exchange for the same or different secondary structural elements (*33*, *34*). The asynchronous correlation spectrum is antisymmetric with respect to the diagonal line, in contrast to the symmetric synchronous spectra. Cross-peaks arise only if the intensity variations change out of phase with respect to each other. In this case, a cross-peak is observed if the change is faster or slower relative to the corresponding spectral coordinates. The sequential order of exchange along the time axis may be determined from Noda's rules (*16*, *17*, *27*). The sign of an asynchronous cross-peak is positive if a change occurs at ν_1 before ν_2. If the sign of the cross-peak is negative, the change at ν_2 occurs before ν_1. The opposite scenario is true if the corresponding cross-peak in the synchronous spectrum is negative.

Two separate asynchronous correlation spectra, covering the spectral regions from 1750 to 1250 cm^{-1} and from 1700 to 1600 cm^{-1}, are shown for each solution of the mAb at pH 2, 4, 6, and 8 (Figures 3 and 4). A total of four cross-peaks were observed from 1700 to 1600 cm^{-1} at pH 2, suggesting four conformational states with differential flexibility. Band assignments and Noda's rules confirm that some β-sheet and disordered structure (1639 cm^{-1}) exchange before a different β-sheet region, possibly consisting of aggregated β-strand with a spectral contribution at 1622 cm^{-1}, based on the negative (1622, 1639) cm^{-1} peak. Similarly, the existence of the (1639, 1690) cm^{-1} cross-peak

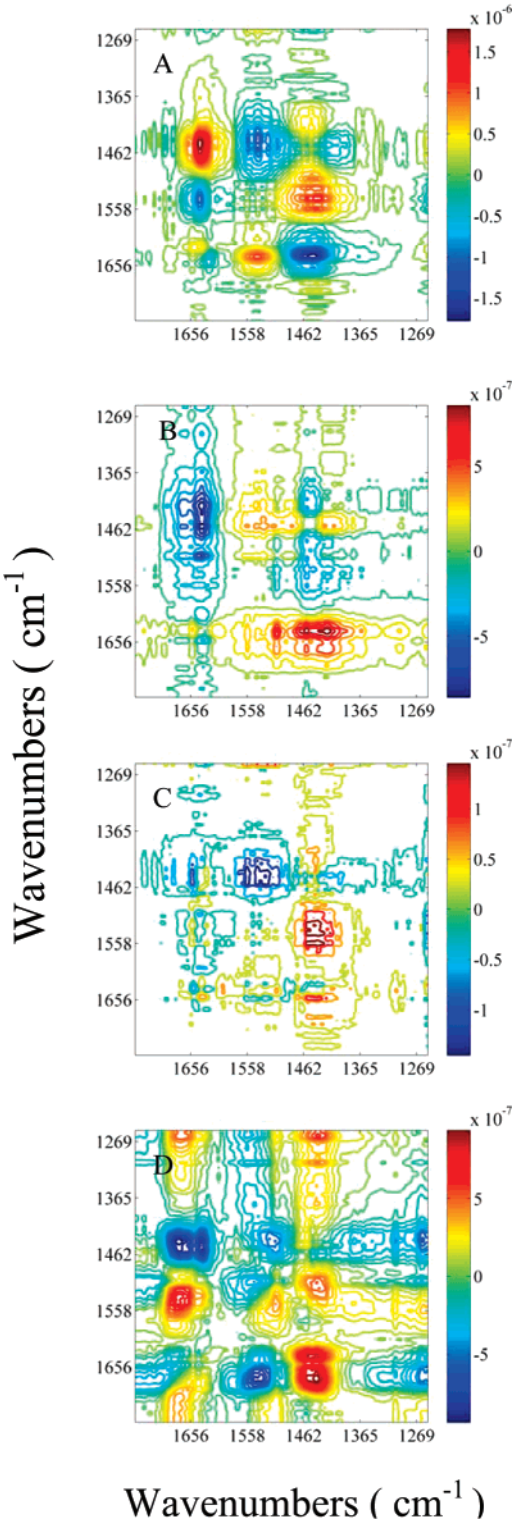

FIGURE 3: Asynchronous 2D IR correlation contour plots corresponding to the frequency range of 1750−1250 cm^{-1} at pH (A) 2, (B) 4, (C) 6, and (D) 8. The scaled intensity change is shown in color.

suggests that another β-sheet region which contributes to the 1690 cm^{-1} band exchanges before the intermediate exchanging β-structure, producing a 1639 cm^{-1} absorption. Finally, the positive peak arising from turns and disordered structure at 1653 cm^{-1} implies that this domain exchanges before the turn structure at 1663 cm^{-1}. When the spectrum is extended to 1750 cm^{-1}, two additional positive cross-peaks are seen at (1639, 1726) and (1652, 1709) cm^{-1}. The two bands at 1726 and 1709 cm^{-1} are presumably due to a C═O stretching vibration of hydrogen-bonded COOH groups of different stengths from Glu and Asp side chains.

The presence of five different regions of differential flexibility is observed for the mAb at pH 4, representing protonated arginine (1604, 1609 cm^{-1}) and conformations of turns and disordered polypeptide (1653 cm^{-1}), and multiple β-sheets [(1691, 1636) and (1670, 1684) cm^{-1}] (Figure 4B). In this analysis, protonated arginine is not considered independently. The following order of exchange is observed at pH 4: protonated arginine side chains (1609 cm^{-1}) > turns/disordered (1653 cm^{-1}) > β-sheet/turns (1670 and 1684 cm^{-1}) ≥ β-sheet (1691 cm^{-1}) > β-sheet (1636 cm^{-1}). The stretching vibration of hydrogen-bonded COOH groups of different stengths from Glu and Asp side chains is again observed at pH 4. Three negative cross-peaks are observed at (1636, 1716), (1636, 1734), and (1664, 1716) cm^{-1}. The band at 1716 cm^{-1} is due to hydrogen-bonded COOH groups, while the 1736 cm^{-1} peak represents free COOH side chains.

The corresponding sign and frequencies of the asynchronous cross-peaks for the mAb at pH 6 are [1634, 1651 (+)], [1626, 1634 (−)], [1601, 1634 (+)], [1647, 1664 (−)], [1627, 1672 (−)], [1634, 1686 (+)], [1614, 1654 (−)], and [1654, 1686 (+)] cm^{-1} (Figure 4C). Approximately seven to eight regions of differential exchange rate are seen at pH 6 corresponding to three β-sheet and single β-sheet/turn, turn, turn/disordered, and disordered regions. Protonated arginine side chains again appear to exchange first (1600 cm^{-1}), followed by β-sheet structure (1634 cm^{-1}), which exchanges much more rapidly when compared to the same structure at pH 4. Following the relatively rapid exchange observed at 1634 cm^{-1}, a region of sheet/turns exchanges before other sheet or extended structure (1626 cm^{-1}) and a combination of sheet/turn/disordered structure (1651−1654 cm^{-1}). The slowest exchanging domain is a β-sheet region (1614 cm^{-1}). The sequence of exchange events for the conformational states corresponding to the turn (1664 cm^{-1}) and disordered (1647 cm^{-1}) region alone was not determined.

Approximately six regions of differential flexibility were deconvoluted in the asynchronous spectrum for the mAb at pH 8. Broad distorted cross-peaks are observed in the pH 8 asynchronous spectrum (Figure 4D). The band near 1634 cm^{-1} exchanges much more readily at pH 8 than at pH 2−4. The β-sheet and disordered regions corresponding to the cross-peak at 1641 cm^{-1} exchange relatively slowly at high pH. The multiple β-sheet segments at pH 8, surprisingly, appear to exchange much more readily when compared to other conformational states. Finally, a peak arising from aspartic and glutamic acid side chains appears relatively resistant to exchange events.

Statistical Correlation Coefficient Maps. Statistical correlation coefficient maps are normalized measures of the strength of the relationship between the spectral intensity variations at two different frequencies. The statistical correlations of spectral intensity variations for the mAb at pH 2, 4, 6, and 8 were calculated (data not shown). These maps appear crowded and complex and are inherently difficult to interpret in terms of changes in protein secondary structure exchange rates based on the Amide I band. Therefore, a matrix of probability values for obtaining a correlation as

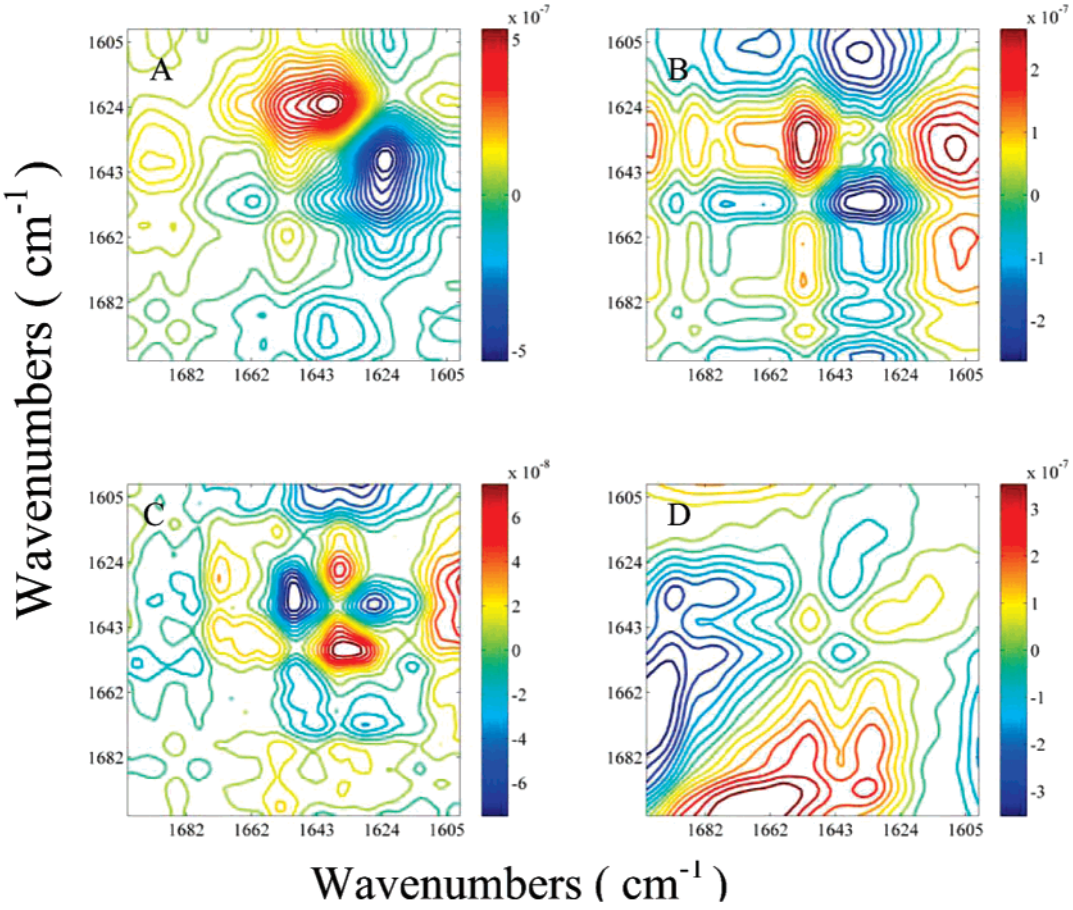

FIGURE 4: Asynchronous 2D IR correlation contour plots corresponding to the Amide I band at pH (A) 2, (B) 4, (C) 6, and (D) 8. The scaled intensity change is shown in color.

large as the observed value by random chance was calculated and used to discriminate among band locations. The propriety of all previous band assignments was confirmed from this matrix of probability values.

Hybrid 2D Spectra. Hybrid two-dimensional correlation spectroscopy enables the visualization of correlations between two separate spectral data matrices (*18*, *24*). Hybrid spectra do not represent the sequence of events between data sets but rather indicate which frequency pairs are responding to the different perturbations in a similar way. Here, asynchronous hybrid spectra are used only for qualitative confirmation of the hybrid synchronous cross-peaks because of their lack of physical meaning (*18*, *23*).

Three positive and two negative peaks are observed in the synchronous hybrid spectra of pH 2 versus pH 4 mAb solutions (Figure 5A). The positive peaks correspond to locations near (1624, 1636), (1624, 1670), and (1664, 1636) cm^{-1}, where the first frequency refers to pH 2 and the second to pH 4. Negative peak coordinates include (1691, 1636) and (1691, 1670) cm^{-1}. A comparison of the mAb at pH 2 (first coordinate) and pH 6 (second coordinate) reveals two positive and two negative peaks at [1624, 1632 (+)], [1663, 1636 (+)], [1622, 1693 (−)], and [1691, 1630 (−)] cm^{-1}, respectively (Figure 5B). Two positive and two negative peaks are observed in the hybrid spectrum between pH 2 and 8 (Figure 5C). The location and sign of each hybrid peak for pH 2 versus pH 8 are as follows: [1624, 1634 (+)], [1663, 1630 (+)], [1651, 1678 (−)], and [1691, 1634 (−)] cm^{-1}. The hybrid correlation spectrum between pH 4 and 6 is composed of three positive broad peaks at (1636, 1630), (1666, 1631), and (1690, 1631) cm^{-1} (Figure 5D). Only two peaks were well-resolved in the synchronous hybrid correlation spectrum between pH 4 and 8 with coordinates at (1636, 1634) and (1670, 1632) cm^{-1} (Figure 5E). Finally, the hybrid spectrum between pH 6 and 8 reveals two positive correlation peaks at (1630, 1634) and (1684, 1832) cm^{-1} (Figure 5F).

Distributions of H−D Exchange Rate Constants

Amide proton exchange rates are dependent on solvent accessibility, protein flexibility, hydrogen bonding, and hydroxide ion concentration (*20*, *21*), among other properties. Exchange rates are greatly diminished for hydrogens that are hydrogen bonded, and every pH unit increase typically increases the observed rate constant 10-fold due to the direct attack of hydroxide ions. Therefore, comparing exchange rates for proteins as a function of pH must be tempered by these considerations.

We have determined the distributions of H−D exchange rate constants from the ratio of the normalized Amide I and Amide II areas for the IgG at pH 2, 4, 6, and 8 (Figure 6). Three distributions of exchange rates, at long, intermediate, and short times, are observed for the mAb at pH 2. In addition to the broad component at longer times, the intermediate distribution at pH 2 is split into three separate components for the mAb at pH 4. The distribution of exchange rates at pH 6 is characterized by a small, fast component, multiple intermediate bands, and a major com-

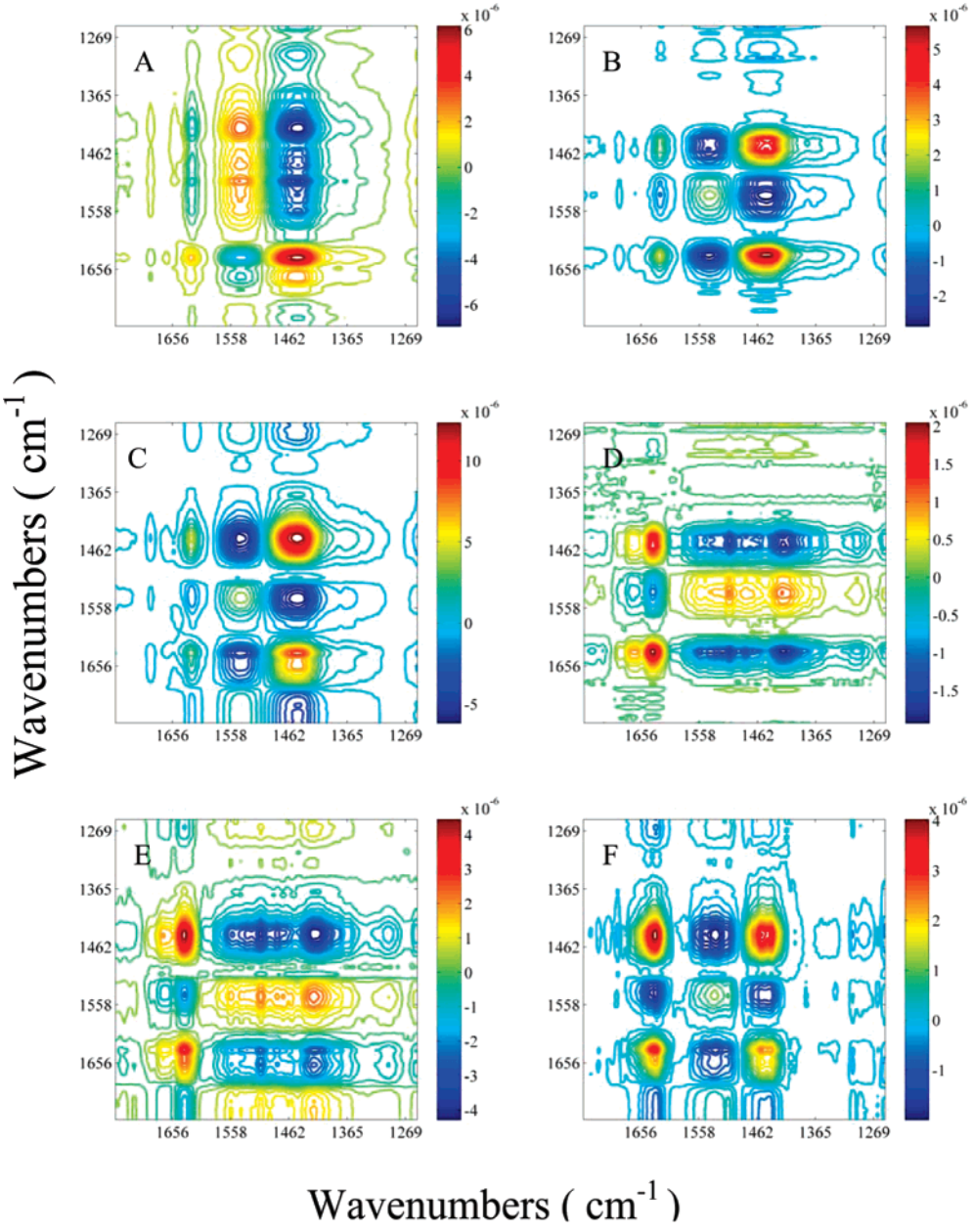

FIGURE 5: Hybrid synchronous 2D IR correlation contour plots corresponding to the frequency range of 1750−1250 cm^{-1} for (A) pH 2 vs pH 4, (B) pH 2 vs pH 6, (C) pH 2 vs pH 8, (D) pH 4 vs pH 6, (E) pH 4 vs pH 8, and (F) pH 6 vs pH 8.

ponent at longer times. Finally, the distribution of rate constants for the IgG at pH 8 is distinguished by four separate resolvable components.

DISCUSSION

Representing protein molecules as ensembles with differential flexibility can provide an improved description of molecular recognition events and protein stability. In this work, we have described the regional flexibility of a monoclonal IgG molecule using H−D exchange and generalized perturbation-based two-dimensional correlation spectroscopy. Multiple overlapping vibrational bands are resolved, and the relative exchange rates of the same and different secondary structural elements are revealed as a function of pH. The number of regions with differential exchange rates, or differential flexibility, as a function of pH varies widely. This work provides direct evidence of multiple regions in diverse molecular environments that may be critically important in the stability of this IgG. The sequence of events leading to immunoglobulin instability and differential flexibility as a function of pH is described.

Immunoglobulin G chains are composed of 12 compact domains of repeating segments approximately 110 amino acids in length. Each domain consists of two β-sheets, which are joined by a disulfide bond. It is known that antibodies are highly flexible molecules and that this plays a role in their ability to bind a diverse number of molecular antigen shapes and sizes. In solution, several aspects of IgG dynamics have been previously studied and include Fab elbow bending, Fab arm waving and rotation, and Fc wagging, among many others. The degree of Fab angular displacement varies widely. The Fab−Fc and Fab−Fab angles range from 66 to 123° and from 115 to 172°, respectively (*35*−*37*). In addition to these motions, collective fluctuations and breathing

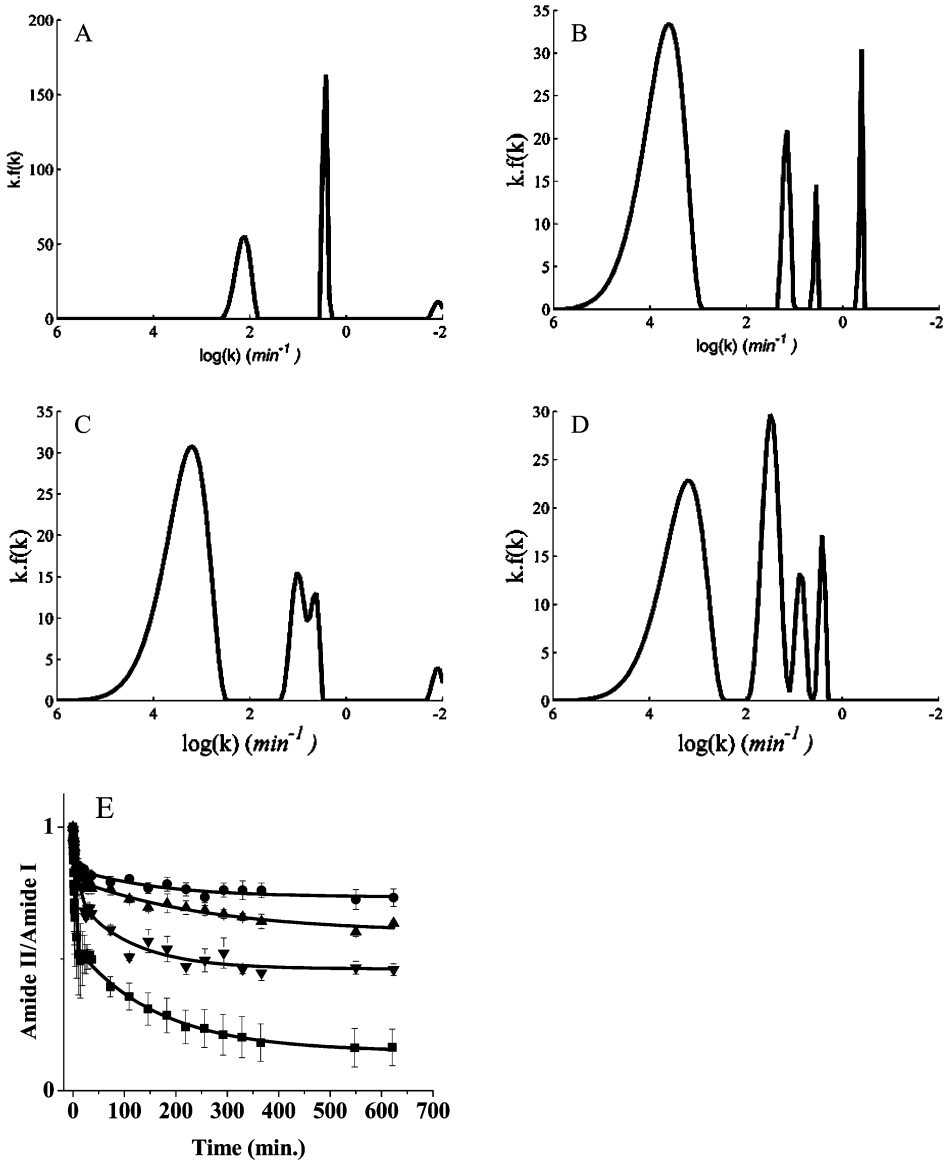

FIGURE 6: Distribution function of the exchange rate constants of the mAb at pH (A) 2, (B) 4, (C) 6, and (D) 8. (E) The ratio of the Amide II to Amide I areas obtained by direct integration for pH 2 (■), 4 (●), 6 (▲), and 8 (▼) IgG solutions. The distribution functions were obtained from the Laplace transformation of the decay curves shown in panel E.

motions of the β-sheet and β-barrel structures characterize immunoglobulin dynamics (*38*). The most flexible IgG structures include the variable regions of the Fab arms and the connecting Fab−Fc hinge region. The hinge region typically consists of three parts (upper, core, and lower hinge) with varying degrees of flexibility and disorder (*37*, *39*, *40*). The upper hinge region allows considerable Fab rotational motions and has greater flexibility compared to the core hinge regions (*41*, *42*). The upper hinge regions of human IgG1 b12, directed against HIV-1 gp120, exhibit the smallest amount of ordered structure, while the lower hinge typically forms extended conformations, although this probably varies among immunoglobulins (*37*, *39*, *40*). In general, the Fc is considered more rigid than the other IgG segments, but differences within each Fc region have been observed. The C_H2 region of the Fc domain manifests higher crystallographic *B*-factors compared to the C_H3 region, suggesting that the C_H2 domain is capable of more dynamic motions than the C_H3 domain (*43*, *44*). On the basis of these considerations, it is clear that many different types of motions, domain interactions, and regional flexibilities contribute to the differential exchange rates observed in this study.

The greatest number of regions with differential exchange rates, and thus differential flexibility, for this IgG is seen at pH 6. Approximately seven to eight, six, five, and four separate regions that exchange with different rates were observed at pH 6, 8, 4, and 2, respectively. Interestingly, the greatest stability, based on measurements of the transition midpoint of thermal unfolding (T_m) (manuscript submitted for publication), follows the same order of differential flexibility. Thus, the extent of conformational heterogeneity or differential flexibility can be hypothesized to be an important determinant of stability for this IgG.

The sequence of events at pH 4 is of special interest. The negative asynchronous cross-peaks at 1636−1716, 1636−1736, and 1664−1716 cm^{-1} suggest that protonation of Glu and Asp COO^- side chains occurs first and presumably initiates changes in structure and flexibility. The observation of cross-peaks at these positions indicates cooperative

conformational changes as previously argued by Murayama et al. (*45*) on the basis of their work with HSA. These changes appear to affect both β-sheet and turns. A second pH-dependent protonation may also be responsible for the differences observed at pH 4. The cross-peaks observed between 1609−1636 and 1604−1666 cm^{-1} suggest that changes in salt bridge formation and/or perhaps protonation of arginine residues with abnormally shifted pK_a values initiates structural alterations involving further cooperative conformational and dynamic changes within β-sheet and turn regions. The fact that these changes are observed between pH 4 and 6, where the greatest change in stability is seen, suggests the presence of pH-dependent, subtle conformational and dynamic changes that result in decreased stability.

Small changes in secondary and tertiary structure are observed for this mAb between pH 2, 4, 6, and 8 on the basis of measurements of near- and far-UV CD as well as intrinsic and extrinsic fluorescence spectroscopy (manuscript submitted for publication). These experiments also suggest that the observed differential flexibility is not the result of major increases in the level of exposure of apolar residues or global unfolding events.

A direct correlation between hydrogen exchange rates and secondary structure integrity does not appear to exist for this mAb at all pH values. In some instances, the vibrational bands representing turns and or disordered structure suggest that they exchange faster than β-sheet regions. This relationship is, however, not always observed. As expected, at pH 4, the less ordered secondary structure is more flexible and exchanges faster. The domains with the greatest flexibility at pH 4 represent states enriched in turns and/or disordered structure, possibly resulting from exchange events in the hinge and/or antigen binding regions. In contrast, at pH 6, a conformation containing more β-sheet (1634 cm^{-1}) is the most flexibile, while the least flexible structure is contained within a different β-sheet region (1614 cm^{-1}). The flexibility of multiple regions at pH 6 is highly variable with certain turns and disordered structure exchanging rapidly and others more slowly. The rapidly exchanging turns and disordered regions may be the result of exchange with the hinge region. In contrast, the relatively rigid regions between, for example, the $C_{H1}-V_H$ or $C_{H2}-C_{H3}$ domains may give rise to the slowly exchanging turns and disordered regions. Furthermore, the β-sheet structure responsible for the 1636 cm^{-1} peak at pH 4 exchanges much more slowly, relative to the other regions, compared to the corresponding feature (1634 cm^{-1}) at pH 6. The major differences in the flexibility of this region suggest some change in the molecular environment. A possibly more important difference in protein dynamics between pH 4 and 6 is observed from states assigned to the turn/disordered region (1653 cm^{-1}). This region appears to be highly flexible at pH 4 but relatively rigid or at least resistant to exchange at pH 6. A more extensive network of both local and long-range interactions is one explanation for the slow or resistant exchange at pH 6. This mAb is much less stable at pH 4 than at pH 6 (manuscript submitted for publication). On the basis of the differences in IgG flexibility, it seems reasonable to propose that these regions are critically involved in maintaining the stability of this IgG.

This high degree of heterogeneity in the differential exchange rates may be an important component of protein stability by compensating for changes in the protein ensemble with a relatively robust network of correlated motions and noncovalent interactions. If the degree of heterogeneity is high, it seems possible that both short- and long-range interactions can provide a stabilizing network of interactions, whereas if predominantly rigid or loose conformations persist, both long- and short-range interactions may not exist. In fact, long range interactions were convincingly shown to stabilize the native ensemble of lysozyme (*4*). Similarly, long-range interactions were shown to critically stabilize the monomeric form of α-synuclein and inhibit oligomerization of this cytotoxic protein which is implicated in Parkinson's disease (*46*). Furthermore, Bouvignies et al. (*2*) have shown that coupled slow dynamics in protein G are communicated over long distances across a four-strand β-sheet through a network of hydrogen bonds. Coupled motions and the network of cooperative stabilizing interactions in proteins are not fully understood, but it is clear that these processes are important for protein function and stability (*2*, *3*, *5*, *6*, *47*).

The resolved peaks in the hybrid correlation maps suggest that the immunoglobulin responds to pH in a similar way at pH 6−8. A different response to pH does appear between pH 2 and 4, however, with multiple negative correlation peaks observed consisting primarily of the 1691 cm^{-1} vibrational band at pH 2 (which can be assigned to turns or β-sheet/turn structure). This may indicate slowing of the exchange rates at pH 2 for this structurally disrupted state, while the other exchange rates are increasing or vice versa. Whatever the case, this structural response to pH changes is unique and is observed at only pH 2 and 4. Other differences may not be resolved because of the limited deconvolution power of the synchronous hybrid correlation method compared to asynchronous methods. To observe differences between pH values, we can simply compare multiple asynchronous spectra.

The overall distribution of exchange rates calculated from the decays of the integrated Amide I and Amide II areas provides further evidence for multiple regions with differential flexibility. These regions cannot necessarily be identified with the well-established β-sheet-rich immunoglobulin 110-residue domains. The major component of the distribution at long times is probably due to the exchange of hydrogens involved in extensive hydrogen bonding networks such as those found within β-structure and/or exposure of deeply buried residues from the protein's core. The distributions of intermediate- and fast-exchanging hydrogens are the result of local fluctuations, and global and subglobal unfolding equilibria. The presence of multiple distributions of intermediate exchange rates may also represent differential structural flexibility and heterogeneity. The fastest exchange processes observed at pH 2 and 6 are characterized by relatively small amplitudes. These fast exchanges may not be well resolved at pH 4 and 8. The fast exchange should be catalyzed to a much greater extent at pH 8. Hydrogen exchange is catalyzed at high pH by direct attack of hydroxide ions which removes amide protons to produce the imidate anion (*20*, *48*). Thus, it seems plausible that this component could not be detected. The intermediate components suggest the greatest mAb flexibility at pH 4. The large amplitudes of the intermediate components at pH 2 and 8 indicate greater flexibility compared to that seen in the IgG at pH 6. These results are in agreement with

measurements of compressibility, expansibility, and state parameter fluctuations measured for this antibody (manuscript submitted for publication).

CONCLUSIONS

This work provides a different perspective concerning immunoglobulin conformational heterogeneity and flexibility. It is probable that both conformational heterogeneity and immunoglobulin dynamics are critically involved in the biological functions and stability of such proteins. Increased conformational flexibility and dynamics should facilitate the recognition and binding of antigens of diverse shape and size. A fourth structural dimension has been proposed to describe proteins on the basis of their conformational heterogeneity and flexibility. This is thought to be critically important for the function of many proteins (*49*). Furthermore, a growing body of evidence suggests that the relationships between protein flexibility and stability are not simply inversely correlated but are better described as a complex interrelationship of the coupling between both rigid and flexible regions. This work provides evidence that immunoglobulins are composed of multiple regions of differential flexibility and conformational heterogeneity, which are differentially perturbed by solution conditions such as pH. It is expected that perturbation-based two-dimensional correlation spectroscopy will provide an improved understanding of the relationships between protein dynamics and stability.

ACKNOWLEDGMENT

The program Kinetics running under Matlab version 7.1 was kindly provided by Dr. E. Goormaghtigh. We also thank S. Morita for use of the program 2Dshige. Finally, we acknowledge the kind gift of the monoclonal antibody from MedImmune, Inc.

REFERENCES

1. Ferreon, J. C., and Hilser, V. J. (2003) Ligand-induced changes in dynamics in the RT loop of the C-terminal SH3 domain of Sem-5 indicate cooperative conformational coupling, *Protein Sci. 12*, 982−996.
2. Bouvignies, G., Bernado, P., Meier, S., Cho, K., Grzesiek, S., Bruschweiler, R., and Blackledge, M. (2005) Identification of slow correlated motions in proteins using residual dipolar and hydrogen-bond scalar couplings, *Proc. Natl. Acad. Sci. U.S.A. 102*, 13885−13890.
3. Hilser, V. J., Dowdy, D., Oas, T. G., and Freire, E. (1998) The structural distribution of cooperative interactions in proteins: Analysis of the native state ensemble, *Proc. Natl. Acad. Sci. U.S.A. 95*, 9903−9908.
4. Klein-Seetharaman, J., Oikawa, M., Grimshaw, S. B., Wirmer, J., Duchardt, E., Ueda, T., Imoto, T., Smith, L. J., Dobson, C. M., and Schwalbe, H. (2002) Long-range interactions within a nonnative protein, *Science 295*, 1719−1722.
5. Bu, Z., Biehl, R., Monkenbusch, M., Richter, D., and Callaway, D. J. (2005) Coupled protein domain motion in Taq polymerase revealed by neutron spin-echo spectroscopy, *Proc. Natl. Acad. Sci. U.S.A. 102*, 17646−17651.
6. Lundstrom, P., Mulder, F. A., and Akke, M. (2005) Correlated dynamics of consecutive residues reveal transient and cooperative unfolding of secondary structure in proteins, *Proc. Natl. Acad. Sci. U.S.A. 102*, 16984−16989.
7. Dangl, J. L., Wensel, T. G., Morrison, S. L., Stryer, L., Herzenberg, L. A., and Oi, V. T. (1988) Segmental flexibility and complement fixation of genetically engineered chimeric human, rabbit and mouse antibodies, *EMBO J. 7*, 1989−1994.
8. Hanson, D. C. (1985) Some theoretical considerations regarding the effects of steric hindrance and intrinsic global coupling on the flexibility of Fc-anchored immunoglobulins, *Mol. Immunol. 22*, 245−250.
9. Hanson, D. C., Yguerabide, J., and Schumaker, V. N. (1981) Segmental flexibility of immunoglobulin G antibody molecules in solution: A new interpretation, *Biochemistry 20*, 6842−6852.
10. Kawata, Y., and Hamaguchi, K. (1991) Use of fluorescence energy transfer to characterize the compactness of the constant fragment of an immunoglobulin light chain in the early stage of folding, *Biochemistry 30*, 4367−4373.
11. Kim, H., Matsunaga, C., Yoshino, A., Kato, K., and Arata, Y. (1994) Dynamical structure of the hinge region of immunoglobulin G as studied by ^{13}C nuclear magnetic resonance spectroscopy, *J. Mol. Biol. 236*, 300−309.
12. Takahashi, H., Suzuki, E., Shimada, I., and Arata, Y. (1992) Dynamical structure of the antibody combining site as studied by ^{1}H-^{15}N shift correlation NMR spectroscopy, *Biochemistry 31*, 2464−2468.
13. Boehm, M. K., Woof, J. M., Kerr, M. A., and Perkins, S. J. (1999) The Fab and Fc fragments of IgA1 exhibit a different arrangement from that in IgG: A study by X-ray and neutron solution scattering and homology modelling, *J. Mol. Biol. 286*, 1421−1447.
14. Ishima, R., and Torchia, D. A. (2000) Protein dynamics from NMR, *Nat. Struct. Biol. 7*, 740−743.
15. Noda, I. (1986) Two-dimensional infrared (2D-IR) spectroscopy of synthetic and biopolymers, *Bull. Am. Phys. Soc. 31*, 520.
16. Noda, I. (1989) Two-Dimensional Infrared Spectroscopy, *J. Am. Chem. Soc. 111*, 8116−8118.
17. Noda, I. (1990) Two-Dimensional Infrared (2D IR) Spectroscopy: Theory and Applications, *Appl. Spectrosc. 44*, 550−561.
18. Wu, Y., Jiang, J. H., and Ozaki, Y. (2002) A New Possibility of Generalized Two-Dimensional Correlation Spectroscopy: Hybrid Two-Dimensional Correlation Spectrsocopy, *J. Phys. Chem. A 106*, 2422−2429.
19. Bai, Y., Sosnick, T. R., Mayne, L., and Englander, S. W. (1995) Protein folding intermediates: Native-state hydrogen exchange, *Science 269*, 192−197.
20. Englander, S. W., Mayne, L., Bai, Y., and Sosnick, T. R. (1997) Hydrogen exchange: The modern legacy of Linderstrom-Lang, *Protein Sci. 6*, 1101−1109.
21. Englander, S. W., Sosnick, T. R., Englander, J. J., and Mayne, L. (1996) Mechanisms and uses of hydrogen exchange, *Curr. Opin. Struct. Biol. 6*, 18−23.
22. Raussens, V., Ruysschaert, J. M., and Goormaghtigh, E. (2004) Analysis of $^{1}H/^{2}H$ exchange kinetics using model infrared spectra, *Appl. Spectrosc. 58*, 68−82.
23. Noda, I., and Ozaki, Y. (2004) *Two-dimensional correlation spectroscopy: Applications in vibrational and optical spectroscopy*, Wiley, Hoboken, NJ.
24. Wu, Y., Yuan, B., Zhao, G., and Ozaki, Y. (2003) Hybrid Two-Dimensional Correlation and Parallel Factor Studies on the Switching Dynamics of a Surface-Stabilized Ferroelectric Liquid Crystal, *J. Phys. Chem. B 107*, 7706−7705.
25. Buchet, R., Wu, Y., Lachenal, G., Raimbault, C., and Ozaki, Y. (2001) Selecting Two-Dimensional Cross-Correlation Functins to Enhance Interpretation of Near-Infrared Spectra of Proteins, *Appl. Spectrosc. 55*, 155−162.
26. Noda, I. (2000) Recent mathematical developments in 2D correlation spectroscopy, in *AIP Conference Proceedings* (Ozaki, Y., and Noda, I., Eds.) pp 2001−2204, American Institute of Physics, New York.
27. Noda, I. (1993) Generalized Two-Dimensional Correlation Method Applicable to Infrared, Raman, and Other Types of Spectroscopy, *Appl. Spectrosc. 47*, 1329−1336.
28. Morita, S. (2004) *2Dshige*, version 1.3, Kwansei-Gakuin University, Nishinomiya, Sanda, and Osaka City, Japan.
29. Goormaghtigh, E. (2007) *KINETICS*, Universite Libre de Bruxelles, Brussels.
30. Knox, D. G., and Rosenberg, A. (1980) Fluctuations of protein structure as expressed in the distribution of hydrogen exchange rate constants, *Biopolymers 19*, 1049−1068.
31. Provencher, S. W. (1982) CONTIN: A General Purpose Constrained Regularization Program For Inverting Noisy Linear Algebraic and Integral Equatins, *Comput. Phys. Commun. 27*, 229−242.
32. Provencher, S. W. (1982) A Constrained Regularization Method for Inverting Data Represented by Linear Algebraic or Integral Equations, *Comput. Phys. Commun. 27*, 213−227.
33. Wu, Y., Murayama, K., and Ozaki, Y. (2001) Two-Dimensional Infrared Spectroscopy and Principle Component Analysis Studies

of the Secondary Structure and Kinetics of Hydrogen-Deuterium Exchange of Human Serum Albumin, *J. Phys. Chem. B 105*, 6251−6259.

34. Nabet, A., and Pezolet, M. (1997) Two-Dimensional FT-IR Spectroscopy: A Powerful Method to Study the Secondary Structure of Proteins Using H-D Exchange, *Appl. Spectrosc. 51*, 466−469.
35. Bongini, L., Fanelli, D., Piazza, F., De Los Rios, P., Sandin, S., and Skoglund, U. (2004) Freezing immunoglobulins to see them move, *Proc. Natl. Acad. Sci. U.S.A. 101*, 6466−6471.
36. Sandin, S., Ofverstedt, L. G., Wikstrom, A. C., Wrange, O., and Skoglund, U. (2004) Structure and flexibility of individual immunoglobulin G molecules in solution, *Structure 12*, 409−415.
37. Saphire, E. O., Stanfield, R. L., Crispin, M. D., Parren, P. W., Rudd, P. M., Dwek, R. A., Burton, D. R., and Wilson, I. A. (2002) Contrasting IgG structures reveal extreme asymmetry and flexibility, *J. Mol. Biol. 319*, 9−18.
38. Chou, K. C. (1985) Low-frequency motions in protein molecules. β-Sheet and β-barrel, *Biophys. J. 48*, 289−297.
39. Saphire, E. O., Parren, P. W., Barbas, C. F., III, Burton, D. R., and Wilson, I. A. (2001) Crystallization and preliminary structure determination of an intact human immunoglobulin, b12: An antibody that broadly neutralizes primary isolates of HIV-1, *Acta Crystallogr. D57*, 168−171.
40. Saphire, E. O., Parren, P. W., Pantophlet, R., Zwick, M. B., Morris, G. M., Rudd, P. M., Dwek, R. A., Stanfield, R. L., Burton, D. R., and Wilson, I. A. (2001) Crystal structure of a neutralizing human IGG against HIV-1: A template for vaccine design, *Science 293*, 1155−1159.
41. Padlan, E. A. (1996) X-ray crystallography of antibodies, *Adv. Protein Chem. 49*, 57−133.
42. Burton, D. R. (1985) Immunoglobulin G: Functional sites, *Mol. Immunol. 22*, 161−206.
43. Harris, L. J., Larson, S. B., Hasel, K. W., Day, J., Greenwood, A., and McPherson, A. (1992) The three-dimensional structure of an intact monoclonal antibody for canine lymphoma, *Nature 360*, 369−372.
44. Burmeister, W. P., Huber, A. H., and Bjorkman, P. J. (1994) Crystal structure of the complex of rat neonatal Fc receptor with Fc, *Nature 372*, 379−383.
45. Murayama, K., Wu, Y., Czarnik-Matusewicz, B., and Ozaki, Y. (2001) Two-Dimensinal/Attenuated Total Reflection Infrared Correlation Spectroscopy Studies on Secondary Structural Changes in Human Serum Albumin in Aqueous Solutions: pH-Dependent Structural Changes in the Secondary Structures and in the Hydrogen Bondings of Side Chains, *J. Phys. Chem. B 105*, 4763−4769.
46. Bertoncini, C. W., Jung, Y. S., Fernandez, C. O., Hoyer, W., Griesinger, C., Jovin, T. M., and Zweckstetter, M. (2005) Release of long-range tertiary interactions potentiates aggregation of natively unstructured α-synuclein, *Proc. Natl. Acad. Sci. U.S.A. 102*, 1430−1435.
47. Mayer, K. L., Earley, M. R., Gupta, S., Pichumani, K., Regan, L., and Stone, M. J. (2003) Covariation of backbone motion throughout a small protein domain, *Nat. Struct. Biol. 10*, 962−965.
48. Berger, A., and Linderstrom-Lang, K. (1957) Deuterium exchange of poly-DL-alanine in aqueous solution, *Arch. Biochem. Biophys. 69*, 106−118.
49. Fragai, M., Luchinat, C., and Parigi, G. (2006) "Four-dimensional" protein structures: Examples from metalloproteins, *Acc. Chem. Res. 39*, 909−917.

BI700645K